Dynamics of Electro-Opto-Mechanical Effects in Swollen Nematic Elastomers

Atsushi Fukunaga,[†] Kenji Urayama,*[,†] Toshikazu Takigawa,[†] Antonio DeSimone,*[,‡] and Luciano Teresi[§]

Department of Materials Chemistry, Kyoto University, Kyoto 615-8510, Japan, SISSA-International School for Advanced Studies, I-34014 Trieste, Italy, and SMFM, Università Roma Tre, I-00146 Rome, Italy

Received July 21, 2008; Revised Manuscript Received October 3, 2008

ABSTRACT: We characterize experimentally the dynamics of the electro-opto-mechanical effect (macroscopic deformation with electro-optical effect) in monodomain liquid crystal elastomers swollen by low molecular mass liquid crystals. The optical and mechanical rise times (in response to field-on) decrease in almost proportion to the square of field strength, while the corresponding decay times (in response to field-off) are nearly independent of field strength. The optical rise and decay times are about 1 order of magnitude smaller than the mechanical ones. We propose a simple model to capture the main features of both static and dynamic aspects of the electro-opto-mechanical effect and use it to interpret the experimental data.

I. Introduction

Liquid crystal elastomers (LCEs) have received considerable attention as interesting stimuli-responsive materials.[1,2] LCEs are rubbery polymer networks with sufficient amounts of rigid mesogenic group to exhibit liquid crystallinity. The coupling of rubber elasticity and liquid crystallinity strongly correlates the macroscopic shape with the alignment of mesogenic molecules. This characteristic of LCEs leads to a rich variety of response behaviors to external stimuli such as temperature, electric fields, mechanical stress, and light.[1]

Low molecular mass liquid crystals (LMLCs) exhibit a large change in optical birefringence in fast response to electric fields—which is called the electro-optical effect—as a result of the director realignment along the field axis. The electro-optical effect is widely employed in many applications of LCs.[3] In the case of LCEs, electric fields are expected to induce a macroscopic deformation originating from the director realignment due to the strong coupling of macroscopic shape and molecular orientational order. In fact, a finite electrically driven deformation has been observed in nematic elastomers swollen in LMLCs.[4−11] The swelling in LMLCs can reduce effectively the elastic modulus—that acts as a strong resistance to dielectric realigning force—without losing the liquid crystallinity. Some recent studies using swollen monodomain LCEs[10,11] with global director orientation were successful in observing simultaneously the macroscopic deformation and the director reorientation under electric fields, i.e., the electromechanical effects coupled to electrooptical effects. An important key to observe clearly this electro-opto-mechanical effect is to use the mechanically unconstrained geometry where the gap between rigid electrodes is larger than the film thickness, because the constraint from rigid electrodes effectively prohibits the macroscopic distortion in the field direction.[12,13] In the constrained geometry, a finite degree of director realignment was observed,[11,14] but it was considerably suppressed.[11]

The static aspects of electro-opto-mechanical effect in swollen monodomain LCEs were studied in detail: the induced strain is proportional to $\sin^2 \theta$, where θ is the rotation angle of director, which is similar to the picture of soft elasticity theory,[1,15−17] and the maximum strain exceeds 15%.[11] The static and dynamic aspects of electro-optical effects of LMLCs and uncrosslinked LC polymers are well understood. In particular, the theories correlate the viscoelastic and dielectric properties of the materials with the dynamic characteristics of the electro-optical effect, i.e., the characteristic times in response to "field-on" and "field-off" which are termed rise and decay times, respectively.[18,19] The LCEs with the coupling of the director rotation and deformation are expected to exhibit interesting dynamics in the electric field responses which significantly differ from LMLCs and uncrosslinked LC polymers. However, the dynamics of electro-opto-mechanical effects of monodomain LCEs still remains to be fully characterized. The response times of swollen LCEs to electric fields were characterized in several experimental studies,[9,14,20] but they reported the dynamics of only either electromechanical[9] or electrooptical effects,[14,20] and in addition, some of their systems employed polydomain LCEs without global director orientation[20] or the constrained geometry where the samples were effectively sandwiched by rigid electrodes.[14] The dynamics of director in LCEs was also investigated by dynamic light scattering[21] and dynamic viscoelastic measurements,[22−24] but in these cases, the amplitude of dynamic response was limited to small perturbations around the equilibrium state. In contrast, the electro-opto-mechanical effects result in large degrees of director rotation far from equilibrium. Studies treating such large amplitude of dynamic director response are limited to the case of relaxation after stretching-induced director rotation.[25]

The understanding of the dynamics of electro-opto-mechanical effects in LCEs is also important from the industrial viewpoint because it provides an important basis of the application of LCEs to electrically driven soft actuators and microelectro-mechanical systems (MEMS). In the present paper, we evaluate experimentally the rise and decay times for the electro-opto-mechanical effects for swollen monodomain LCEs as a function of the imposed field strength. We also propose a simple model to interpret the experimental data. The model correlates the response times with the dielectric and viscoelastic properties of the swollen LCEs.

II. Experimental Section

Side-chain type nematic elastomers were prepared by the methods discussed in the previous paper.[26] The mixtures of the reactive

* To whom correspondence should be addressed. E-mail: urayama@rheogate.polym.kyoto-u.ac.jp (K.U.); desimone@sissa.it (A.D.).
[†] Kyoto University.
[‡] SISSA-International School for Advanced Studies.
[§] Università Roma Tre.

10.1021/ma801639j CCC: $40.75
Published on Web 11/11/2008

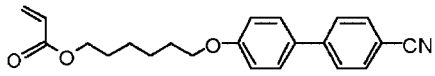

Figure 1. Chemical structure of the employed reactive mesogen.

Table 1. Sample Characteristics

sample	cross-linker concentration (mol %)	5CB content (vol %)	d_g (μm)	T_{NI}[a] (°C)
S-LCE-7	7	78	43	51
S-LCE-10	10	73	40	49

[a] In the swollen state.

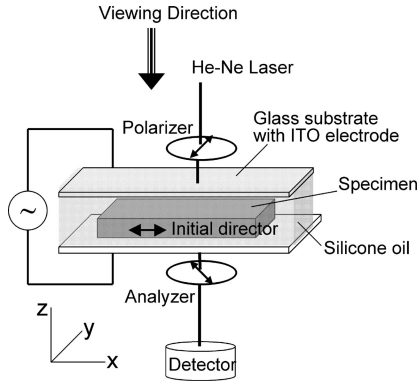

Figure 2. Experimental setup for the observation of electro-optical and electro-mechanical effects.

mesogenic monomer (Figure 1), miscible nematogenic solvent (4-*n*-hexyloxy-4′-cyanobiphenyl), cross-linker (1,6-hexanediol diacrylate), and photoinitiator (Irgacure 784) were sandwiched by two glass plates whose surfaces were coated with rubbed polyimide layer to induce planar mesogen alignment. The mixing molar ratio of the reactive mesogen and nematic solvent was 1:1. The cross-linker concentration in the feed, which is indicated by *X* in the sample code S-LCE-*X*, was 7 or 10 mol%. The cell gap was 40 μm. After the photopolymerization by irradiation of light of wavelength 526 nm, the resultant gel film was carefully removed from the glass plates. The unreacted monomers and solvent were washed out from the specimen by swelling in dichloromethane. The swollen gel film was gradually deswollen by using mixtures of dichloromethane and methanol with various mixing ratios. The fully dried films were allowed to swell in the low molecular mass LC, 4-*n*-pentyl-4′-cyanobiphenyl (5CB), until the swelling was equilibrated. The solvent contents and thicknesses of the elastomers in the equilibrium swollen states are summarized in Table 1. The solvent and nematic elastomers are miscible in the fully swollen state because the swollen elasotmers exhibit a single phase transition temperature.[27] The transition temperature of each swollen sample (T_{NI}) is also shown in Table 1.

The swollen gel films in the shape of squares with edge length of ca. 1 mm were placed between two glass plates having transparent ITO electrodes with a controlled gap of 50 μm. The cell gap was set to be larger than the gel thickness so that the specimen could have no mechanical constraint from the rigid electrodes. The cell was filled with transparent silicone oil which is a nonsolvent for the swollen elastomers. AC fields with a square wave of a frequency of 1 kHz were applied with a function generator. The effective optical birefringence (Δn) in the $x-y$ plane was evaluated by measuring the transmittance of the incident beam using the optical geometry in Figure 2. The deformation process after applying and removing the fields was observed using an optical microscope equipped with a high speed video camera Photron FASTCAM-512PCI. The time dependence of strain γ ($\gamma = \Delta l/l_0$ where Δl and l_0 are the dimensional change and initial dimension, respectively) was estimated by the video analysis.

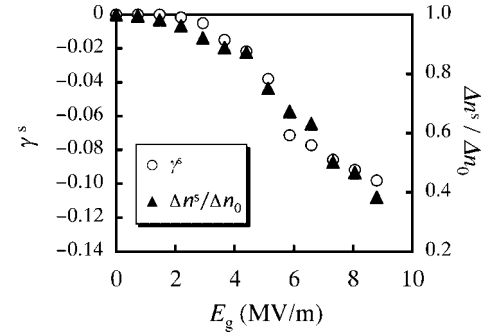

Figure 3. Strain along the initial director and effective optical birefringence in the steady state as a function of E_g for S-LCE-7.

III. Results and Discussion

A. Static aspects of Electro-Opto-Mechanical Effects. Figure 3 shows the strain along the initial director and effective birefringence in the steady state ($t \rightarrow \infty$) as a function of E_g for S-LCE-7. The quantity E_g is the nominal field strength acting on the gel specimen defined as

$$E_g = \frac{\epsilon_s}{\epsilon_s d_g + \epsilon_g d_s} V_0 \tag{1}$$

where ϵ_g, ϵ_s, d_g, and d_s are the dielectric constants along the field axis and layer thicknesses for the gels (g) and silicone oil (s), respectively. For simplicity, we approximate here ϵ_g by the dielectric constant normal to the long axis of 5CB. The characteristics in the steady state were studied in detail in our previous papers.[11] In this section, we briefly summarize the main features of the static aspects of this phenomenon. The electric field induces a rotation of the director in the $x-z$ plane: the director departs from its initial x-direction (see Figure 2) and eventually attains a steady state characterized by the angle θ it forms with respect to the horizontal. The corresponding deformation is characterized by a shortening in the x-direction, an extension in the z-direction, and a nonappreciable dimensional variation in the y-direction (the axis of rotation of the director); moreover, the deformation process appears to be isochoric (constant volume). The absence of dimensional change along the director rotation axis evidently indicates that this deformation is governed by the rotation of director. We denote hereafter γ_x and its steady state value γ_x^s as γ and γ^s, respectively. The steady state strain $|\gamma^s|$ increases with increasing E_g, and it reaches 10% at high field strengths. The effective birefringence in the steady state (Δn^s) decreases with increasing E_g, and it reduces to ca. 40% of the initial value (Δn_0) at the highest E_g in this study. A threshold to induce a finite change in each quantity is observed, and these thresholds ($E_{g,c} \approx 2.1$ MV/m) are almost identical.

B. Dynamic Aspects of Electro-Opto-Mechanical Effects. Figure 4 shows the typical examples of the time dependencies of γ and Δn in response to the imposition and removal of the fields. Each quantity evolves in time and attains a steady state which depends on E_g, and it recovers to the initial value after the removal of the field. We simply evaluate the characteristic times for the responses to the field imposition and removal (designated as rise and decay times, respectively) as the time periods needed for 70% of total change. A movie file for the electromechanical responses can be found in the Supporting Information. Note that the experimental conditions including the sample in the movie are different from those in Figure 4 (see the Supporting Information Section at the end of this paper for the details).

Figure 5 displays the rise times $\tau_{on}^{\Delta n}$ and τ_{on}^{γ} regarding the optical and mechanical effects as a function of E_g. In the small E_g region of $E_g < 3$ MV/m, τ_{on}^{γ} could not be evaluated with

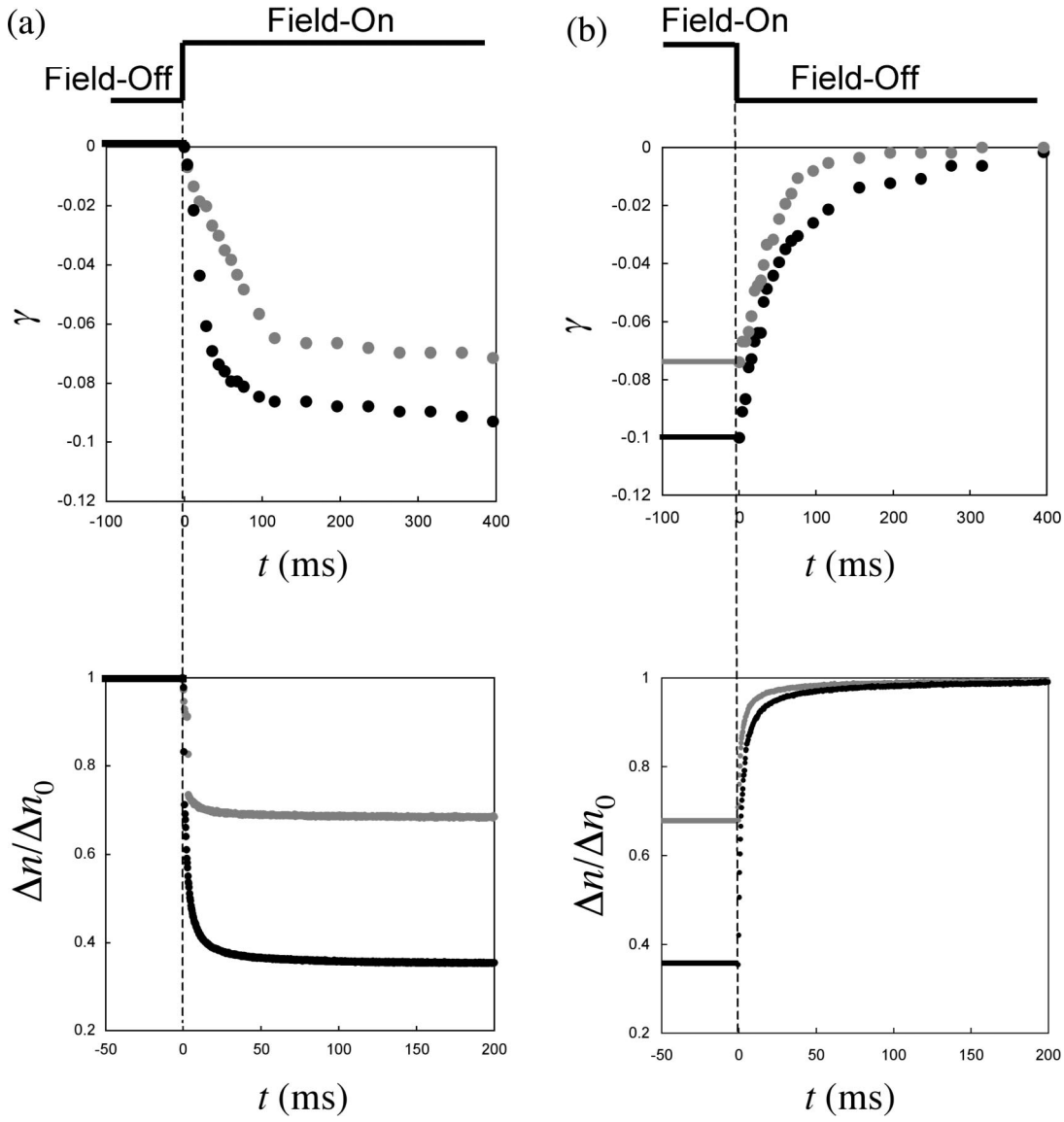

Figure 4. Time dependencies of strain and birefringence after (a) applying and (b) removing the fields for S-LCE-7. The black and gray symbols represent the data at $E_g = 8.8$ and 5.9 MV/m, respectively.

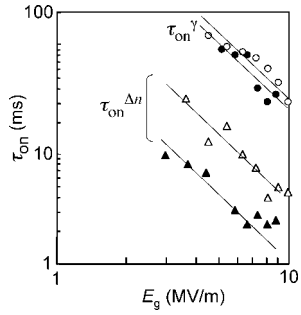

Figure 5. Optical and mechanical rise times as a function of E_g. The filled and open symbols depict the data of S-LCE-7 and S-LCE-10, respectively. The slope of the lines is 2.

sufficient accuracy because of the small induced strains of $\gamma^s < 0.03$. The values of τ_{on}^{γ} range from 20 to 100 ms. The values of τ_{on}^{γ} for S-LCE-7 are smaller than those for S-LCE-10, but the difference is considerably small. For S-LCE-7, $\tau_{on}^{\Delta n}$ are less than 10 ms in the E_g range examined while $\tau_{on}^{\Delta n}$ for S-LCE-10 at each E_g is a few times larger than that for S-LCE-7. Both $\tau_{on}^{\Delta n}$ and τ_{on}^{γ} become smaller with increasing E_g, and their dependencies are approximated by $\tau_{on}^{\Delta n} \sim E_g^{-2}$ and $\tau_{on}^{\gamma} \sim E_g^{-2}$.

In the high E_g region of $E_g > 7$ MV/m, $\tau_{on}^{\Delta n}$ for S-LCE-7 appears to become constant at around a few milliseconds, because it will correspond to the lower limit of the response time for the frequency (1 kHz) of the imposed field. The saturation of $\tau_{on}^{\Delta n}$ at the same level (a few milliseconds) is also observed for the pure 5CB at sufficiently high fields with a frequency of 1 kHz. For any E_g, the optical response is considerably faster than the mechanical response: $\tau_{on}^{\Delta n}$ is about 1 order of magnitude smaller than τ_{on}^{γ}.

Figure 6 shows the E_g dependence of the decay times $\tau_{off}^{\Delta n}$ and τ_{off}^{γ} regarding the optical and mechanical responses. Both decay times are independent of E_g: $\tau_{off}^{\Delta n} \approx 4$ ms and $\tau_{off}^{\gamma} \approx 50$ ms for S-LCE-7; $\tau_{off}^{\Delta n} \approx 7$ ms and $\tau_{off}^{\gamma} \approx 60$ ms for S-LCE-10. As in the case of τ_{on}, the mechanical decay time is about 1 order of magnitude larger than the optical one. The ratio of τ^{γ} to $\tau^{\Delta n}$ for any E_g appears to be constant, regardless of field imposition or removal: $\tau_{on}^{\gamma}/\tau_{on}^{\Delta n} \approx \tau_{off}^{\gamma}/\tau_{off}^{\Delta n} \approx a$ where $a \approx 20$ for S-LCE-7 and $a \approx 10$ for S-LCE-10. It should be noted that the considerably faster response of the optical effect is not due to the independent motion of the nematic solvent inside the gels. In the planar-alignment cell whose gap is similar to the gel thickness (25 μm), the decay time of the pure 5CB is a few seconds, which is 3 orders of magnitude larger than that of

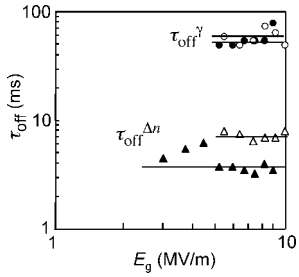

Figure 6. Optical and mechanical decay times as a function of E_g. The filled and open symbols depict the data of S-LCE-7 and S-LCE-10, respectively.

the gels. This indicates that the solvent inside the gels moves together with the gel matrix, and that the recovering force in swollen nematic elastomers is by far stronger than that (Frank elasticity) in pure liquid crystals.

C. Interpretation of the Experimental Data Using a Minimal Model. In order to interpret the experimental results, we consider the simplest model for the dynamics of nematic gels under an applied electric field consistent with the observations reported above. The measured static electro-opto-mechanical response calls for a free-energy coupling orientational order, gel deformations, and dielectric properties in the regime of large director rotations. With such a free-energy at hand, a classical scheme to formulate the evolution equations governing the dynamics of the system is based on the balance between free-energy release rate and rate of viscous dissipation. In both of these two modeling steps, we can rely on several contributions from the existing literature,[22−25] as discussed below in more detail.

The free-energy of the system is assumed to be

$$F = F_F + F_{el} + F_g \tag{2}$$

where the three summands are the Frank energy, the electrostatic energy, and the gel elasticity energy, respectively. The Frank curvature elasticity energy is

$$F_F = \frac{1}{2}\int_B k_F |\nabla n(x)|^2 dx \tag{3}$$

where B is the region of space occupied by the gel, $n = (\cos\theta, 0, \sin\theta)$ is the nematic director, and k_F is Frank constant. Notice that we are assuming that n is always confined to the plane $x-z$ defined by the initial director orientation and the one of the applied electric field (see Figure 2). The electrostatic energy associated with an electric potential ϕ is

$$F_{el} = -\frac{1}{2}\varepsilon_0\int_B (\varepsilon_a(\nabla\phi(x)\cdot n(x))^2 + \varepsilon_g|\nabla\phi(x)|^2)\,dx - \frac{1}{2}\varepsilon_0\int_{\Omega/B}\varepsilon_s|\nabla\phi(x)|^2\,dx \tag{4}$$

where Ω/B denotes the part of the cell outside the sample and occupied by silicon oil, ϵ_0 denotes the free space permittivity, while ε_{par}, ε_g, $\varepsilon_a = \varepsilon_{par} - \varepsilon_g$, and ε_s are the dielectric constants given in Table 2. Notice that eq 4 is the total electrostatic energy including the one needed to maintain a constant voltage difference V_0 across the cell (see eq 3.67 in ref 18). Finally, the elastic energy of the gel is

$$F_g = \int\left(f_{an}(n(x)) + \frac{G}{2}|e_u(x) - e_0(n(x))|^2\right)dx \tag{5}$$

where

$$f_{an}(n) = \frac{k_1}{2}\sin^2\theta + \frac{k_2}{4}\sin^4\theta \tag{6}$$

is an anisotropic energy density representing a restoring torque driving the director n toward its direction n_0=(1,0,0) at cross-linking, and G is the shear modulus setting the energy scale for the rubber elasticity term, namely, the second summand in eq 5. There, e_u is the linear strain with components

$$(e_u)_{ij} = \frac{1}{2}\left(\frac{\partial u_i}{\partial x_j} + \frac{\partial u_j}{\partial x_i}\right) \tag{7}$$

with $u_i(x)$ the ith component of the displacement at the point x of the gel with respect to its reference configuration (chosen as the one the specimen would take in the high temperature isotropic phase) and x_j the jth coordinate of x. Finally, $e_0(n)$ is the stress-free state associated with n, which we assume to be a volume-preserving uniaxial extension along n. This is given by the following matrix valued function of n or, equivalently, of the angle θ

$$[e_0(n)] = \begin{bmatrix} \frac{3}{2}g\left(\cos^2\theta - \frac{1}{3}\right) & 0 & \frac{3}{2}g\sin\theta\cos\theta \\ 0 & -\frac{g}{2} & 0 \\ \frac{3}{2}g\sin\theta\cos\theta & 0 & \frac{3}{2}g\left(\sin^2\theta - \frac{1}{3}\right) \end{bmatrix} = [e_0(\theta)] \tag{8}$$

with $g > 0$ a material parameter controlling the magnitude of spontaneous distortion in the gel. In particular, the length change along the x direction due to an unconstrained rotation of the director n in the $x-z$ plane is described by $(e_u)_{11} = (e_0(\theta))_{11}$. Thus, a rotation from $\theta = 0$ to an arbitrary angle θ is accompanied by a strain γ_x given by

$$\gamma_x(\theta) = \frac{L_x(\theta) - L_x(0)}{L_x(0)} = \frac{(e_0(\theta))_{11} - (e_0(0))_{11}}{1 + (e_0(0))_{11}} = -\frac{3}{2}\frac{g}{1+g}\sin^2\theta \tag{9}$$

Introducing the parameter $k = L_x(0°)/L_x(90°)$ as in ref 11, eq 9 can be rewritten as $\gamma_x(\theta) = (k^{-1} - 1)\sin^2\theta$, so that the relations between g and k are $g = 2(k-1)/(k+2)$.

We remark that the expression for rubber elasticity in eq 5 is modeled, just for simplicity, after the elastic energy for an isotropic incompressible material with shear modulus G and natural (stress-free) state e_0. More realistic expressions, taking into account the anisotropy introduced by n and n_0 are possible; see, e.g., refs 22 and 23. In fact, in the absence of specific measurements of the several different elastic moduli of the gel compatible with material symmetry, G should be understood simply as a measure of the energy scale associated with mechanical deformations of the sample. For what concerns the anisotropy energy driving n to n_0, an expression similar to eq 6 has been considered in ref 25 and in eq 8.30 of ref 1. We also remark explicitly that we are assuming throughout that rigid body rotations are negligible.

Table 2. Material Parameter Values Used in the Model

symbol	value	description
d_g	43 μm	thickness of gel sample B
H_Ω	50 μm	thickness of cell Ω
d_s	7 μm	thickness of silicon oil layer
g	0.12	magnitude of spontaneous strain
G	2×10^3 J/m^3	gel shear modulus
k_F	10^{-11} J/m	Frank constant
k_1	300 J/m^3	first anisotropy constant
k_2	6000 J/m^3	second anisotropy constant
$(\eta_n)^{-1}$	8.6×10^{-2} m^3/(J s)	director mobility
η_g	50 (J s)/m^3	gel viscoelastic modulus
ϵ_0	8.85×10^{-12} F/m	free-space permittivity
ϵ_s	2.0	silicon oil dielectric constant
ϵ_g	7.0	gel dielectric constant (perpendicular to n)
ϵ_{par}	18.5	gel dielectric constant (parallel to n)

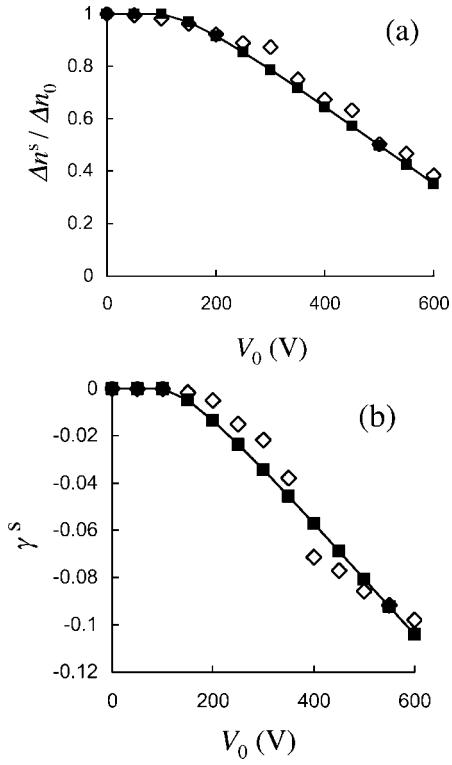

Figure 7. Numerical (filled symbols) versus experimental (open symbols) results for (a) effective optical birefringence and (b) strain along the initial director in the steady state as a function of E_g for S-LCE-7.

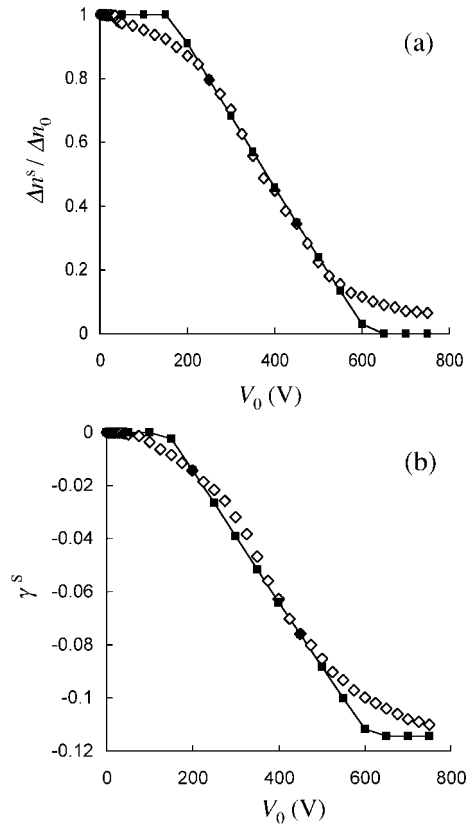

Figure 8. Numerical (filled symbols) versus experimental (open symbols) results for (a) effective optical birefringence and (b) strain along the initial director in the steady state as a function of E_g for a different sample but with the same cross-linker concentration as S-LCE-7. The experimental data were from ref 4.

The dynamics of the system is assumed to be governed by electrostatics, viscoelasticity of the gel, and rotational viscoelasticity of the director. In abstract form, these partial differential equations read as

$$0 = \frac{\delta F}{\delta \phi} \tag{10}$$

$$\eta_g \mathrm{div}\left(\frac{\partial}{\partial t} e_u\right) = -\frac{\delta F}{\delta u} \tag{11}$$

$$\eta_n \frac{\partial}{\partial t} n \times n = -\frac{\delta F}{\delta n} \times n \tag{12}$$

where $\delta F/\delta\phi$, $\delta F/\delta u$, and $\delta F/\delta n$ are, respectively, the variational derivatives of the free-energy with respect to ϕ, u, and n. In these equations, η_g is the viscoelastic modulus of the gel, η_n^{-1} is the director mobility, and the vector product with n has been introduced in eq 12 to take into account the pointwise constraint $|n(x)| = 1$. We remark that more general expressions are usually considered for the viscous terms,[22−25] just as noted above for the elastic terms. In fact, in the regime of small director rotations, the viscoelastic terms in our model can be obtained as the isotropic limit of those considered in ref 23 by setting $\mu = G$, $\eta = \eta_g$, $\gamma_1 = \eta_n$, and $\gamma_2 = 0$. The reason for our choice is not an implicit statement that the effects of anisotropy on the elastic and viscous coefficients are negligible but, once again, the limited experimental evidence at our disposal, which makes the calibration of a larger set of material constants unfeasible.

In the geometry of interest here, eqs 10−12 simplify considerably and in what follows we only discuss this special case (see, however, ref 28 for a discussion of the structure of these equations in the general case). Since the sample is unconstrained, the director n, the strain e_u, and the strain rate $\partial/\partial t\ e_u$ are spatially uniform. Moreover, given the high aspect ratio of both gel sample and cell, the electric field $-\nabla\phi$ is essentially parallel to z and given by the following expressions

$$-\nabla \phi_g = \frac{1}{d(\theta)} V_0;\ d(\theta) = d_g + \frac{\varepsilon_g + \varepsilon_a \sin^2 \vartheta}{\varepsilon_s} d_s \tag{13}$$

$$-\nabla \phi_s = \frac{\varepsilon_g + \varepsilon_a \sin^2 \theta}{\varepsilon_s d_g + (\varepsilon_g + \varepsilon_a \sin^2 \theta) d_s} V_0 \tag{14}$$

holding far away from the lateral edges in the gel and in the silicon oil filling the cell, respectively. Here $d(\theta)$ represents an effective thickness of the cell, which depends on the orientation of n. We recover eq 1 from eq 13 when $\theta = 0$.

Since strain rates and stresses are spatially uniform, eq 11 reduces to the system of ordinary differential equations

$$\eta_g \frac{\mathrm{d}}{\mathrm{d}t} e_u = -G(e_u - e_0(n)) \tag{15}$$

We recall that the director rotates in the plane x-z defined by n_0 and by the electric field, and we assume that only the 11, the 33, and the 13 strain components are nontrivial. Therefore, the torque balance eq 12 governing the orientation of n becomes

$$\eta_n \frac{\mathrm{d}}{\mathrm{d}t} \vartheta = T_G + T_{an} + T_\phi \tag{16}$$

where the elastic torque T_G, the restoring torque T_{an}, and the electrostatic torque T_ϕ are given by

$$T_G = 3Gg\{(e_u)_{13}(\cos^2 \theta - \sin^2 \theta) + [(e_u)_{33} - (e_u)_{11}] \sin \theta \cos \theta\} \tag{17}$$

$$T_{an} = -(k_1 + k_2 \sin^2 \theta) \sin \theta \cos \theta \tag{18}$$

$$T_\phi = \varepsilon_0 \varepsilon_a \left(\frac{V_0}{d(\theta)}\right)^2 \sin\theta \cos\theta \tag{19}$$

At steady state, eq 15 reduces to the matrix identity

$$e_u \equiv e_0(n) \tag{20}$$

In turn, this implies that $T_G = 0$, as it can be easily checked using eq 8 in eq 17. Then it follows that, at steady state, eq 16 reduces to

$$0 = T_{an} + T_\phi \tag{21}$$

Solving eq 21 for θ, we determine the equilibrium value θ^s of θ as a function of V_0. Moreover, using eq 9 we can express the equilibrium value γ^s of γ as a function of V_0, i.e., $\gamma^s = \gamma^s(\theta^s(V_0))$. These equilibrium values of θ and γ are shown in Figure 7 through plots of $\cos^2\theta^s$ and of γ^s as functions of the applied voltage V_0. These are compared with the corresponding experimental plots showing steady values of effective optical birefringence and deformation for S-LCE-7. When the birefringence is sufficiently small relative to the principal refractive indices, the reduced effective optical birefringence $\Delta n/\Delta n_0$ (where Δn_0 is the birefringence in the state without field) is well approximated as

$$\frac{\Delta n}{\Delta n_0} \approx \cos^2\theta \tag{22}$$

The validity of this assumption for the present materials was shown in our previous paper.[11] Figure 7 shows a threshold voltage V_c for the onset of director rotation, and a maximum value of $|\gamma^s|$ for large applied voltages. The threshold voltage V_c is the minimal voltage required for the existence of roots θ of eq 21 different from integer multiples of 0 and $\pi/2$. With positive k_1 and k_2, this is given by

$$V_c = \sqrt{\frac{k_1}{\varepsilon_0 \varepsilon_a}} \frac{\varepsilon_s d_g + \varepsilon_g d_s}{\varepsilon_s} \tag{23}$$

Using eq 1, this can be expressed as a critical value of the nominal electric field in the gel given by

$$E_{g,c} = \sqrt{\frac{k_1}{\varepsilon_0 \varepsilon_a}} \tag{24}$$

Equation 24, which is one of the main results of this paper, links the threshold for director reorientation to the values of intrinsic material parameters. The threshold is thus determined by field strength rather than voltage, and it is directly related to the strength of the memory of the director orientation at cross-linking. The maximum value of $|\gamma^s|$ is obtained from eq 9 with $\theta = \pi/2$. With the material parameters we use, we obtain the values $V_c = 115$ V, $E_{g,c} = 1.8$ MV/m, and $|\gamma^s|_{max} = 3g/[2(1+g)] \approx 0.16$.

Figure 8 shows the superposition of steady state values of $\cos^2\theta$ and γ_x coming from theory and experiment for a different sample,[11] for which experimental values do saturate at high voltages, in agreement with the predictions of the model. The values of the material parameters that fit the experimental data for this case are slightly different from those given in Table 2 for sample S-LCE-7. They are $g = 0.0825$, $k_1 = 650$ J/m^3, $k_2 = 4100$ J/m^3, $d_g = 34$ μm, and $d_s = 6$ μm. As compared to S-LCE-7, the sample in Figure 8 is thinner and confined in a cell with a narrower gap but it has the same cross-linker concentration. The data of S-LCE-7 at the high voltages of $V_0 > 600$ V could not be obtained due to electric short circuit during the measurements.

Turning now to the model predictions concerning the dynamics of the system (eqs 15 and 16), we compute the time evolution of $\cos^2\theta(t)$ and $\gamma(t)$ following from switching on and off voltages at $V_0 = 400$ V and $V_0 = 600$ V. These are given in Figure 9. It is worth mentioning here that, for the selection of material parameter values to be used in the calculations, we first tune the material parameters g, k_1 and k_2 to fit the steady data of Figure 7. Then, using these values, we tune the viscosity parameters η_g, η_n^{-1} and the shear modulus G to fit the dynamic data of Figure 9.

Finally, following the definition in section III.B, we determine the values of $\tau_{on}^{\Delta n}$, τ_{on}^{γ}, $\tau_{off}^{\Delta n}$, and τ_{off}^{γ} resulting from the theory

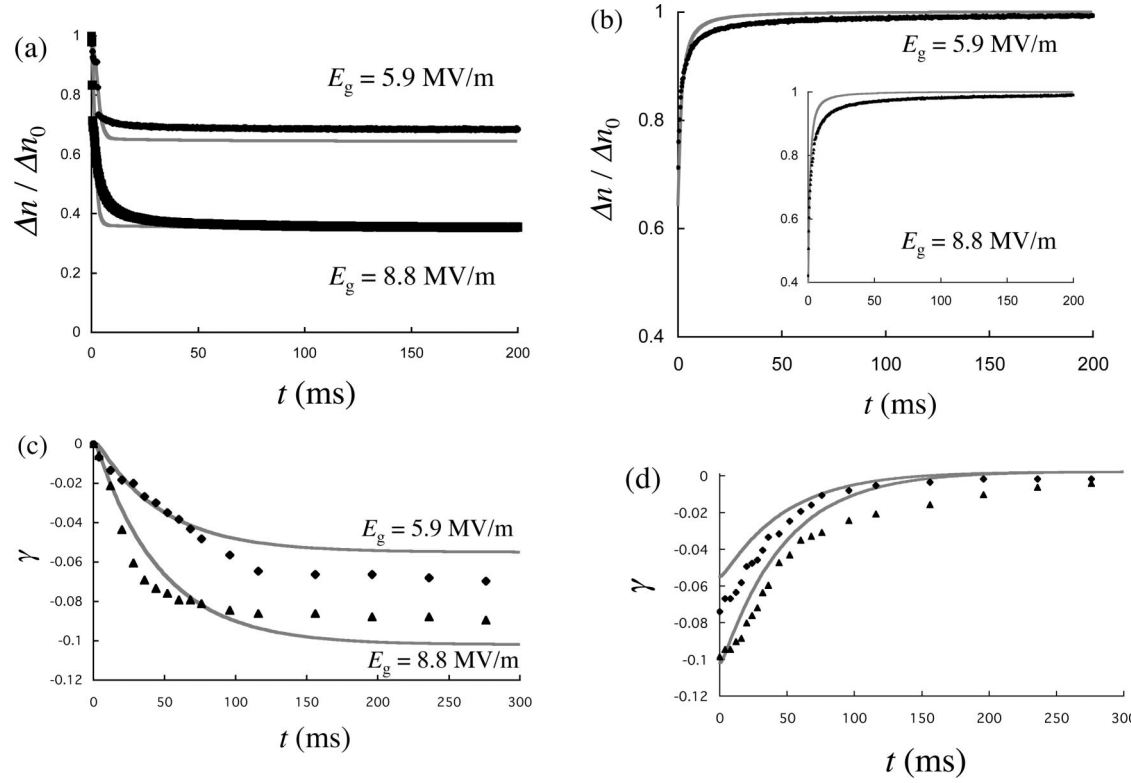

Figure 9. Numerical (gray solid lines) versus experimental (dots) results for the time dependencies of birefringence after (a) applying and (b) removing the fields of $E_g = 5.9$ and 8.8 MV/m for S-LCE-7. The corresponding dependencies of strain are shown in parts c and d.

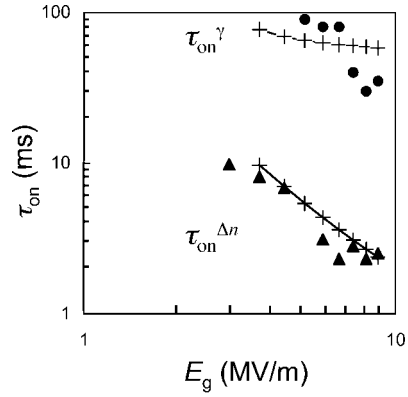

Figure 10. Numerical (crossed symbols) versus experimental (filled symbols) results for the optical and mechanical rise times as a function of E_g.

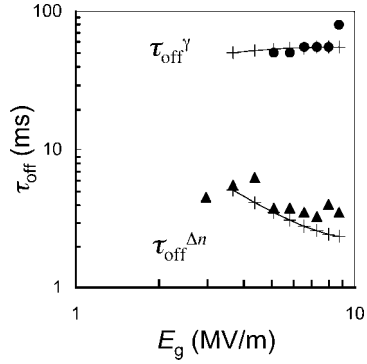

Figure 11. Numerical (crossed symbols) versus experimental (filled symbols) results for the optical and mechanical decay times as a function of E_g.

in response to various values of the applied voltage V_0. These are given in Figures 10 and 11 as functions of the nominal electric field in the gel E_g, defined in eq 1. The $\tau_{on}^{\Delta n} \sim E_g^{-2}$ behavior exhibited by the experimental values is well captured by the model. By contrast, the $\tau_{on}^{\gamma} \sim E_g^{-2}$ behavior exhibited by at least one of the samples in Figure 5 is not reproduced by the model, which only shows a weak dependence of τ_{on}^{γ} on E_g (see the discussion below for an explanation of this discrepancy). In Figure 11, we compare the model predictions and experimental data regarding the decay times. The parameter values employed are the same as those in Figure 10. The theory reproduces well the almost no E_g dependence of $\tau_{off}^{\Delta n}$ and τ_{off}^{γ} as well as a finite difference in magnitude between them.

Some further insight in the predictions of the model can be gained by linearizing the evolution eq 16 around $\theta = 0$, and assuming that director evolution is infinitely faster than the evolution of elastic displacements. This approximation scheme yields some coarse estimates of $\tau_{on}^{\Delta n}$, τ_{on}^{γ}, $\tau_{off}^{\Delta n}$, and τ_{off}^{γ}, valid for small θ, which may be useful in applications. When the voltage is turned on, we thus imagine that the director evolves with e_u frozen at its initial value $e_0(\theta = 0)$. Using this value in eq 16 leads to

$$\eta_n \frac{d}{dt}\theta = \left(-\frac{9}{2}gG - k_1 + \varepsilon_0\varepsilon_a \frac{{\varepsilon_s}^2}{(\varepsilon_s d_g + \varepsilon_g d_s)^2} {V_0}^2\right)\theta \qquad (25)$$

Solving eq 25, we obtain

$$\theta(t) = \theta_0 \exp\left(\frac{K_{on}}{\eta_n} t\right) \qquad (26)$$

where θ_0 is a small initial pretilt, necessary to escape from the unstable equilibrium $\theta = 0$ and

$$K_{on} = K_{on}(V_0) = \varepsilon_0\varepsilon_a \frac{{\varepsilon_s}^2}{(\varepsilon_s d_g + \varepsilon_g d_s)^2} {V_0}^2 - k_1 - \frac{9}{2}gG \qquad (27)$$

It follows from the definition of $\tau_{on}^{\Delta n}$ that $\theta(\tau_{on}^{\Delta n}) = \theta_0 + 0.7(\theta^s - \theta_0)$. Using the values in Table 2, we obtain

$$\tau_{on}^{\Delta n} \cong \ln\left(0.3 + 0.7\frac{\theta^s}{\theta_0}\right)\frac{\eta_n}{K_{on}(V_0)} \qquad (28)$$

In view of eq 27, eq 28 leads to a $\tau_{on}^{\Delta n} \sim {V_0}^{-2}$ behavior and hence to $\tau_{on}^{\Delta n} \sim E_g^{-2}$.

When the voltage is turned off, we assume that the director evolves with e_u frozen at its initial value, which is now the one corresponding to the steady director orientation under applied voltage $e_0(\theta = \theta^s)$. Substituting this into eq 16 leads to

$$\eta_n \frac{d}{dt}\theta = \left(-\frac{9}{2}gG - k_1\right)\theta \qquad (29)$$

Solving eq 29, we obtain

$$\theta(t) = \theta^s \exp\left(-\frac{K_{off}}{\eta_n} t\right) \qquad (30)$$

where

$$K_{off} = k_1 + \frac{9}{2}gG \qquad (31)$$

and, in turn, using the values in Table 2,

$$\tau_{off}^{\Delta n} \cong -\ln(0.3)\frac{\eta_n}{K_{off}} \cong 10 \text{ ms} \qquad (32)$$

Applying the approximation scheme discussed above to estimate the rise and decay times of the elastic displacements, we solve the evolution equation (15) by assuming that the director has already relaxed to a steady equilibrium value. This leads to solving

$$\eta_g \frac{d}{dt} e_u(t) = -G(e_u(t) - e_0(\theta^s)), \quad e_u(t)|_{t=0} = e_0(\theta = 0) \qquad (33)$$

when the field is on, and to

$$\eta_g \frac{d}{dt} e_u(t) = -G(e_u(t) - e_0(0)), \quad e_u(t)|_{t=0} = e_0(\theta = \theta^s) \qquad (34)$$

when the field is off. With the values in Table 2, we thus obtain

$$\tau_{on}^{\gamma} \cong \tau_{off}^{\gamma} \cong -\ln(0.3)\frac{\eta_g}{G} \cong 30 \text{ ms} \qquad (35)$$

As noted above, experiments confirm the independence of τ_{off}^{γ} from E_g, not the one of τ_{on}^{γ}. The discrepancy stems from the fact that, in reality, the characteristic response times of gel and director are not as widely separated as it is assumed in the model.

As a final remark we compare our results on swollen LCE gels with the data on rotational viscosity coefficients in dry LCEs obtained by Schoenstein et al. via dynamic light scattering studies.[21] The relaxation times $\tau_{off}^{\Delta n}$ (see Figure 6 above) and τ (see Figure 5 in ref 21) in the two systems are not widely different. Our swollen gel is elastically much softer than the dry elastomer (our k_1 is 2 orders of magnitude smaller than the estimated value for D_1 in ref [21]). As a consequence, our viscosity coefficient η_n (which satisfies $\tau_{off}^{\Delta n} \approx \eta_n/k_1$ from eqs 31 and 32 above) is much smaller than η_{loss} which is estimated from $\tau^{-1} = D_1/\eta_{loss}$ (eq 25 in ref 21).

IV. Conclusions

We have presented measurements of the dynamic response of swollen monodomain nematic elastomers to applied electric fields. Most of the results are consistent with a simple model

based on an elastic energy attracting the director to its direction at cross-linking, electrostatic interactions tending to align the director with the applied electric field, and a viscous dissipation mechanisms opposing director and deformation changes which uses linear viscous coefficients.

By fitting the theoretical response to the experimental data we have provided estimates for the values of the key material parameters governing the dynamic response of swollen nematic gels to applied electric fields. We have also obtained some coarse estimates for the characteristic response times $\tau_{on}^{\Delta n}$, τ_{on}^{γ}, $\tau_{off}^{\Delta n}$, and τ_{off}^{γ}, valid for small θ, which may be useful in applications.

Among the challenges for continuing work, we quote the following. From the experimental side, it would be interesting to try to measure the complete set of elastic moduli and viscosities allowed by the anisotropy of the material, and to probe for the existence of a larger set of characteristic response times depending on the loading conditions, as envisaged in ref 23. However, a direct measurement of the elastic constants has been until now problematic, both because of the extreme softness (with nominal shear modulus G of order of a few kPa) and the small thickness of the samples. From the theoretical side, we note that although the small strain approximation seems appropriate to model the experimental data reported in this paper, with measured strains not exceeding 10%, larger deformations may be expected in general. Thus, an interesting challenge is the development of a fully nonlinear theory of the electro-opto-mechanical response of nematic gels, by including electrostatic interactions in the framework proposed in ref 15 and analyzed in refs 29−33.

Acknowledgment. This work was partly supported by the Grant-in-Aid on Priority Area "Soft Matter Physics" (No. 19031014) and that for Scientific Research (B) (No. 16750186) from the Ministry of Education, Culture, Sports, Science and Technology (MEXT) of Japan. This research was also supported in part by the Global COE Program "International Center for Integrated Research and Advanced Education in Materials Science" (No. B-09) of MEXT of Japan, administrated by the Japan Society for the Promotion of Science. K.U. appreciates the travel expense support from the "Executive program of scientific and technological cooperation between Italy and Japan" administrated by MEXT of Japan. L.T. thanks SISSA for continued hospitality and support.

Supporting Information Available: A mpeg movie file demonstrating an electrically driven deformation for a 26 μm-thick sample with a cross-linker concentration of 4 mol % which is confined in a 40 μm-thick cell filled with 5CB. The 5CB content in the sample is 82 vol %. The AC field with an amplitude of 750 V and a frequency of 1 kHz (normal to the screen) is imposed normally to the initial director (x) orientation (horizontal direction). The field induces a shortening of ca. 20% in the x-direction with a nonappreciable dimensional variation in the vertical (y) direction. The sample dimensions recover to the initial values after the removal of the field. The movie runs in real-time. Natural light was used for the clear observation of the deformation. Note that the experimental conditions including the sample in this movie are not identical with those in this paper. This material is available free of charge via the Internet at http://pubs.acs.org.

References and Notes

(1) Warner, M.; Terentjev, E. M. *Liquid Crystals Elastomers (Revised Edition)*; Clarendon Press: London, 2007.
(2) Urayama, K. *Macromolecules* **2007**, *40*, 2277–2288.
(3) Colings, P. J.; Hird, M., *Introduction of Liquid Crystals, Chemistry and Physics*; Taylor & Francis: London, 1997.
(4) Zentel, R. *Liq. Cryst.* **1986**, *1*, 589–592.
(5) Barnes, N. R.; Davis, F. J.; Mitchell, G. R. *Mol. Cryst. Liq. Cryst.* **1989**, *168*, 13–25.
(6) Kishi, R.; Suzuki, Y.; Ichijo, H.; Hirasa, O. *Chem. Lett.* **1994**, 2257–2260.
(7) Huang, C.; Zhang, Q. M.; Jakli, A. *Adv. Funct. Mater.* **2003**, *13*, 525–529.
(8) Urayama, K.; Kondo, H.; Arai, Y. O.; Takigawa, T. *Phys. Rev. E* **2005**, *71*, 051713.
(9) Yusuf, Y.; Huh, J. H.; Cladis, P. E.; Brand, H. R.; Finkelmann, H.; Kai, S. *Phys. Rev. E* **2005**, *71*, 061702.
(10) Urayama, K.; Honda, S.; Takigawa, T. *Macromolecules* **2005**, *38*, 3574–3576.
(11) Urayama, K.; Honda, S.; Takigawa, T. *Macromolecules* **2006**, *39*, 1943–1949.
(12) Terentjev, E. M.; Warner, M.; Bladon, P. *J. Phys. II* **1994**, *4*, 667–676.
(13) Terentjev, E. M.; Warner, M.; Meyer, R. B.; Yamamoto, J. *Phys. Rev. E* **1999**, *60*, 1872–1879.
(14) Chang, C. C.; Chien, L. C.; Meyer, R. B. *Phys. Rev. E* **1997**, *56*, 595–599.
(15) Warner, M.; Bladon, P.; Terentjev, E. M. *J. Phys. II* **1994**, *4*, 93–102.
(16) Olmsted, P. D. *J. Phys. II* **1994**, *4*, 2215–2230.
(17) Verwey, G. C.; Warner, M. *Macromolecules* **1995**, *28*, 4303–4306.
(18) de Gennes, P. G.; Prost, J., *The Physics of Liquid Crystals*, 2nd ed.; Oxford University Press: New York, 1993.
(19) Stewart, I. W., *The Static and Dynamic Continuum Theory of Liquid Crystals*; Taylor & Francis: London, 2004.
(20) Cho, D. U.; Yusuf, Y.; Hashimoto, S.; Cladis, P. E.; Brand, H. R.; Finkelmann, H.; Kai, S. *J. Phys. Soc. Jpn.* **2006**, *75*, 083711.
(21) Schonstein, M.; Stille, W.; Strobl, G. *Eur. Phys. J. E* **2001**, *5*, 511–517.
(22) Terentjev, E. M.; Warner, M. *Eur. Phys. J. E* **2001**, *4*, 343–353.
(23) Fradkin, L. J.; Kamotski, I. V.; Terentjev, E. M.; Zakharov, D. D. *Proc. R. Soc. London Series A* **2003**, *459*, 2627–2642.
(24) Martinoty, P.; Stein, P.; Finkelmann, H.; Pleiner, H.; Brand, H. R. *Eur. Phys. J. E* **2004**, *14*, 311–321.
(25) Teixeira, P. I. C.; Warner, M. *Phys. Rev. E* **1999**, *60*, 603–609.
(26) Urayama, K.; Arai, Y. O.; Takigawa, T. *Macromolecules* **2005**, *38*, 3469–3474.
(27) Urayama, K.; Arai, Y. O.; Takigawa, T. *Macromolecules* **2005**, *38*, 5721–5728.
(28) DeSimone, A.; DiCarlo, A.; Teresi, L. *Eur. Phys. J. E* **2007**, *24*, 303–310.
(29) DeSimone, A. *Ferroelectrics* **1999**, *222*, 275–284.
(30) DeSimone, A.; Dolzmann, G. *Physica D* **2000**, *136*, 175–191.
(31) DeSimone, A.; Dolzmann, G. *Arch. Rat. Mech. Anal.* **2002**, *161*, 181–204.
(32) Conti, S.; DeSimone, A.; Dolzmann, G. *J. Mech. Phys. Solids* **2002**, *50*, 1431–1451.
(33) Conti, S.; DeSimone, A.; Dolzmann, G. *Phys. Rev. E* **2002**, *66*, 061710-1–8.

MA801639J